ACS APPLIED NANO MATERIALS

www.acsanm.org Article

Omnidirectionally Stretchable Metal Films with Preformed Radial Nanocracks for Soft Electronics

Seong Won Kim, Siyoung Lee, Daegun Kim, Seung Goo Lee,* and Kilwon Cho*

Cite This: *ACS Appl. Nano Mater.* 2020, 3, 7192−7200 Read Online

ACCESS | Metrics & More | Article Recommendations | SI Supporting Information

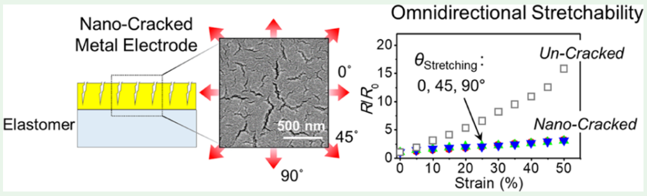

ABSTRACT: Flexible and stretchable conductive thin films are required for the development of soft electronics; however, few existing films satisfy the requirements for both electrical/mechanical performances and process practicability. This study describes a simple approach to fabricate omnidirectionally and highly stretchable nanocracked metal thin films on thiolated elastomeric substrates by exploiting the eruption of a residual solvent contained in an elastomeric substrate during metal thermal evaporation. Also, the effects of residual solvent content in the substrate on the crack topography of a metal thin film and its resultant stretching characteristics are investigated. The solvent content in the range of 0.2−0.3 wt % facilitates the formation of radial nanocracks with a high density of small cracks, which is most suitable for dissipating omnidirectional tensile stress. When a strain of 100% is applied to the elastomeric substrate, the electrical resistance of the radially nanocracked stretchable Au film increases only slightly compared to that of the uncracked Au film. Furthermore, the film shows high stability under repeated stretching cycles and harsh mechanical conditions, enabling its application to stretchable interconnects for a flexible light-emitting diode array. This method provides an effective approach to obtain high-quality thin metal electrodes for use in flexible and wearable devices.

KEYWORDS: *stretchable electrode, residual stress, thermal evaporation, nanocracks, microcracks, metal thin films, omnidirectional stretchability, stretchable interconnects*

■ INTRODUCTION

Stretchable and conductive thin-film electrodes[1] have attracted considerable attention because of increasing demand for soft electronics such as flexible displays,[2,3] flexible batteries,[4] soft actuators,[5] and wearable sensors.[6−11] However, conductive thin films fabricated on elastomeric substrates can easily lose their electrical performance in a stretched state because of macroscale cracks caused at a low strain (1−2%) by the difference in the elastic modulus and Poisson's ratio between the film and the substrate.[12] To overcome this limitation, researchers have introduced deformable structures onto films, such as wrinkle,[13,14] mesh,[15,16] or serpentine[17] structures. These structures help distribute the applied stress by allowing out-of-plane or in-plane deformation at their edges, which enables the film to move relatively freely in the stretched state. Such stretchability is promoted by more twisted or more meandering structures such as three-dimensional serpentine structures.[18] However, such overly deflected structures have a low spatial density,[19] which might preclude intricate device designs.[20] In addition, a complex and laborious process such as prestraining,[21] lift-off,[22] or transfer[23] is required to fabricate such deformable structures, which further reduces their applicability. Furthermore, most previously reported stretchable electrodes have been reported to exhibit direction-dependent stretching characteristics because of the limited deformation of their aligned structures.[24] Hence, for the commercialization of future soft electronics, a new method should be developed to fabricate omnidirectionally stretchable thin films while ensuring process simplicity and high spatial density.

Metals have been widely used as a representative material for conductive thin films because they can be deposited through a commercially available vacuum deposition process and because they exhibit excellent electrical conductivity. To improve the stretchability of metal thin films, nanoscale crack formation is a promising method because it involves a simple fabrication process and features a high degree of integration. When the nanoscale cracks are aligned unidirectionally, the film has been found to enable ultrahigh sensitivity to external strain and vibration. However, these architectures lack structures that can deflect cracks or retard their propagation, so it is hard to be used for stretchable applications.[25,26] Otherwise, radially (i.e., tri-branched or Y-shaped) nanocracked metal films exhibit high and omnidirectional stretchability because the propagating cracks can be easily deflected and retarded irrespective of the stretching direction; these films therefore show promise as deformable

Received: June 4, 2020
Accepted: June 17, 2020
Published: June 17, 2020

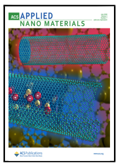

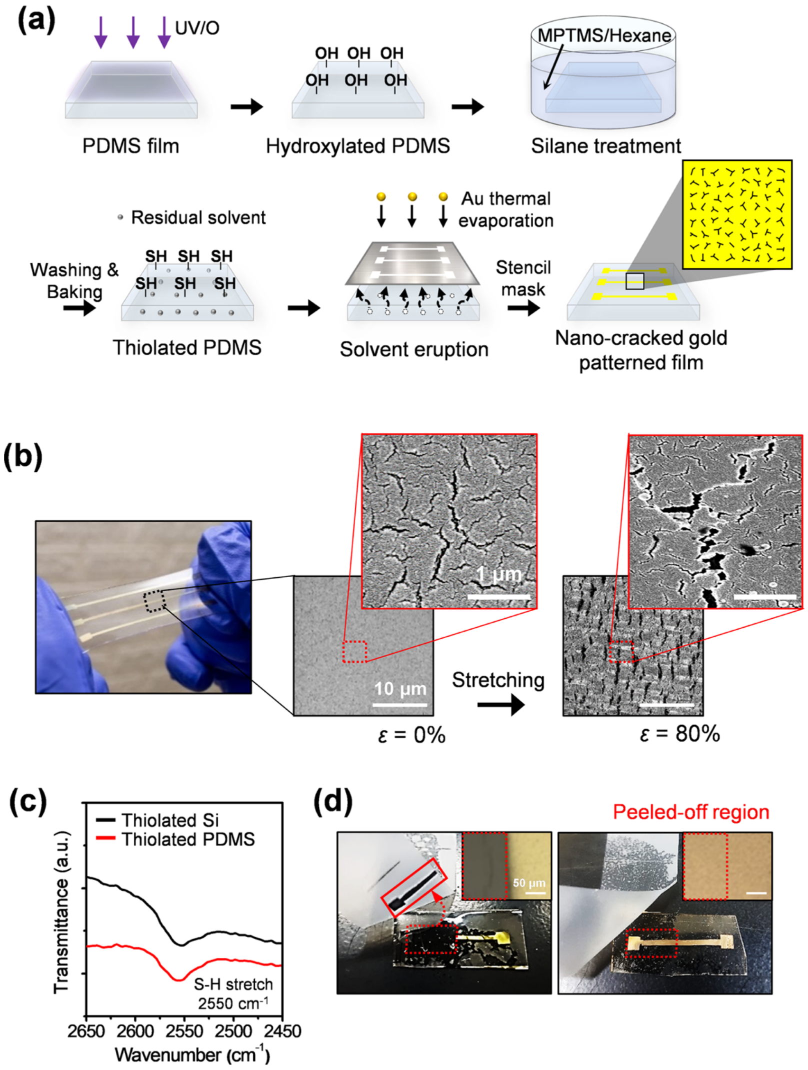

Figure 1. Fabrication of nanocracked stretchable gold film. (a) Fabrication process for the nanocracked stretchable gold film (NC-GF). (b) Photograph of the patterned NC-GF and the corresponding SEM images of the NC-GF in an unstretched state and under 80% tensile strain. (c) FT-IR spectra of the thiolated Si wafer and the PDMS film. (d) Photographs showing the peel-off test for gold films deposited on untreated PDMS (left) and thiolated PDMS (right). (Insets show the corresponding optical microscopy (OM) images; red lines represent the regions where the tape test was conducted.)

structures for stretchable electrodes.[27,28] Stretchable thin metal films with radial nanocracks have been fabricated using a Cr adhesion layer between a Au thin film and a compliant substrate; this layer can apply sufficient thermal stress to initiate cracking of the thin metal film during thermal evaporation.[29] However, the factors that control the geometries of cracks in deposited metal films are not well understood, so unintentional macroscale defects can occur under poorly controlled conditions, and the relationship between the crack geometry and the stretching characteristics of films remains unclear.[30] Recently, there was an attempt to fabricate stretchable cracked Au films by inducing intrinsic stress of the films through high-rate deposition.[31] However, this approach has limitations that intrinsic stress is sensitive to the type of metals and to the surface conditions of substrates.

Here, we introduce a simple and controllable method for fabricating highly and omnidirectionally stretchable, robust electrodes on elastomeric substrates, where the electrode consists of a thermally evaporated Au film on which radial nanocracks are formed. This method exploits the solvent-eruption phenomenon that occurs during thermal evaporation of metals on an elastomer that contains the residual solvent. The eruption of solvent imparts additional strain to the deposited metal film, resulting in the development of a radial nanocrack morphology that resembles ground cracking induced by volcanic eruption.[32] To increase the stretchability and robustness of the film, we controlled the nanocracks' geometry by changing the amount of residual solvent within the elastomer and sequentially introduced a Au−S bond between the Au film and the underlying elastomeric substrate by treating the substrate surface with a thiol group-ended silane. The optimized radially nanocracked gold film (NC-GF) exhibited excellent electrical characteristics in all stretching directions; it exhibited a moderate proportional increase in the electrical resistance (R/R_0) of 6.0 at a strain ε of 100% and operated stably after repeated stretching cycles. This simple process for the fabrication of Au patterns makes the NC-GF easily adaptable to two-dimensional serpentine structures. Serpentine-patterned NC-GF interconnects exhibited an R/R_0 of 2.8 under 100% strain and were fully operational even after being subjected to severe mechanical

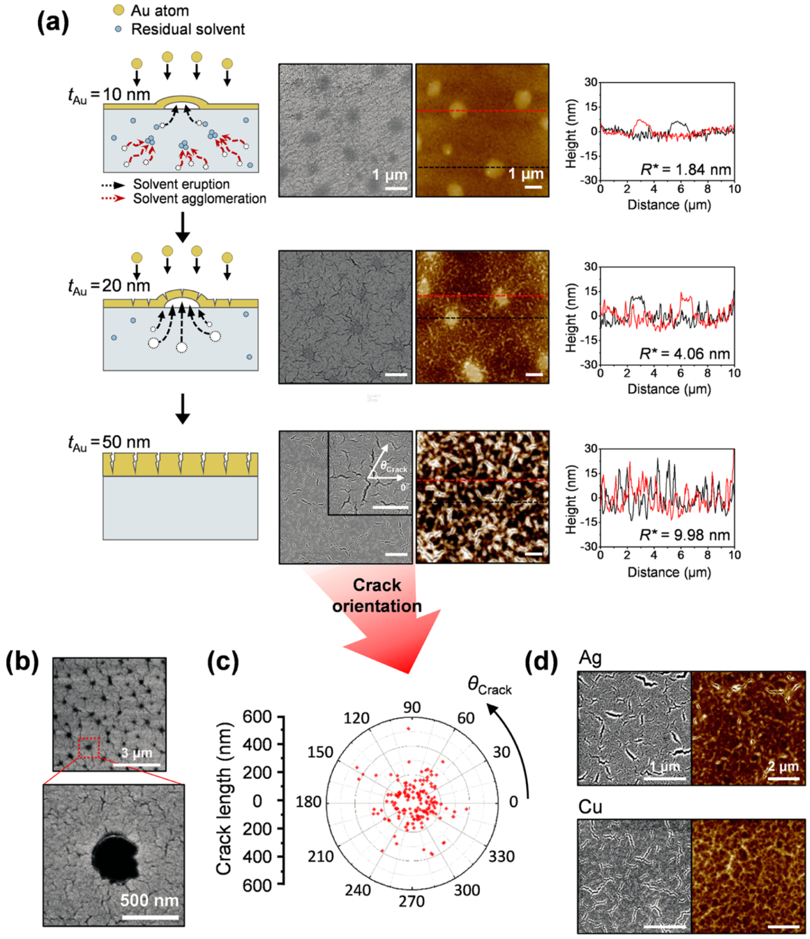

Figure 2. Proposed mechanism for the formation and propagation of nanocracks. (a) Schematic drawing of the proposed mechanism for the formation of nanocracks on the gold film by solvent eruption-induced stress (σ_{erupt}) and correlated morphologies (SEM, AFM) and height profile of NC-GFs according to the thickness of the deposited gold film. (b) Crater-like morphology of the gold film deposited on PDMS with an excessive amount of residual solvent. (c) Orientation angle and length distribution of nanocracks on the NC-GF (t_{Au} = 50 nm). (d) Morphologies (SEM, AFM) of the nanocracked Ag and Cu films.

deformation (80% tensile or compressive strain and 10,000 repeated cycles). Because of their superior stretchability and robustness, the NC-GFs exhibited excellent stability when used as stretchable interconnects for a light-emitting diode (LED) array.

■ RESULTS AND DISCUSSION

Fabrication of the Nanocracked Metal Film. For practical applications, stretchable and mechanically robust metal films should be fabricated using a simple method that requires neither complex processing nor laborious experimental conditions. In our method, a stretchable Au film was achieved through the introduction of nanoscale radial cracks via a solvent-eruption phenomenon that occurs on the solvent-containing elastomer during metal thermal evaporation. Simultaneously, the robustness was improved by treatment of the surface of an elastomer such as poly(dimethylsiloxane) (PDMS) with a thiol group-ended silane to increase interfacial adhesion through Au−S bonding. Because the solvent incorporation into PDMS and the surface silane treatment are conducted in a single-step solvent-based process, the stretchability and robustness of the deposited metal thin film can be improved simply and simultaneously.

First, a UV−ozone-treated PDMS film (thickness ≈ 250 μm) was immersed in an organic solvent containing 3-mercaptopropyl trimethoxysilane (MPTMS) (Figure 1a). Because the following high-vacuum environment in a vacuum chamber is a harsh condition for the solvent to reside within the matrix, hexane was used as a solvent considering its high miscibility with PDMS (Table S1 and Figure S1).[33] Then, a stencil pattern mask was placed on the PDMS film, and a Au layer with a thickness of 50 nm was thermally evaporated onto it. A scanning electron microscopy (SEM) image of the Au film shows that nanocracks with a length of 100 to 500 nm were uniformly formed on its surface, with no macroscale cracks observed (Figure 1b). These nanocracks function as deformable geometries that can dissipate the applied stress and deflect the propagating cracks in the film and are therefore expected to help maintain the film's connective morphologies when it is stretched. Despite the presence of nanocracks, the sheet resistance (3.7 Ω/sq) of the NC-GF was similar to that of an uncracked gold film (UC-GF) (3.3 Ω/sq) because the cracked geometries are comparatively too small to affect the conducting path of the film (Figure S2). Thiolation of the PDMS surface was confirmed on the basis of the similarity between the S−H stretching peak of MPTMS deposited onto the PDMS and the silicon wafer in Fourier transform infrared (FT-IR) spectra (Figure 1c). Because of the strong Au−S interaction, the results of the peel-off test (Figure 1d) and the

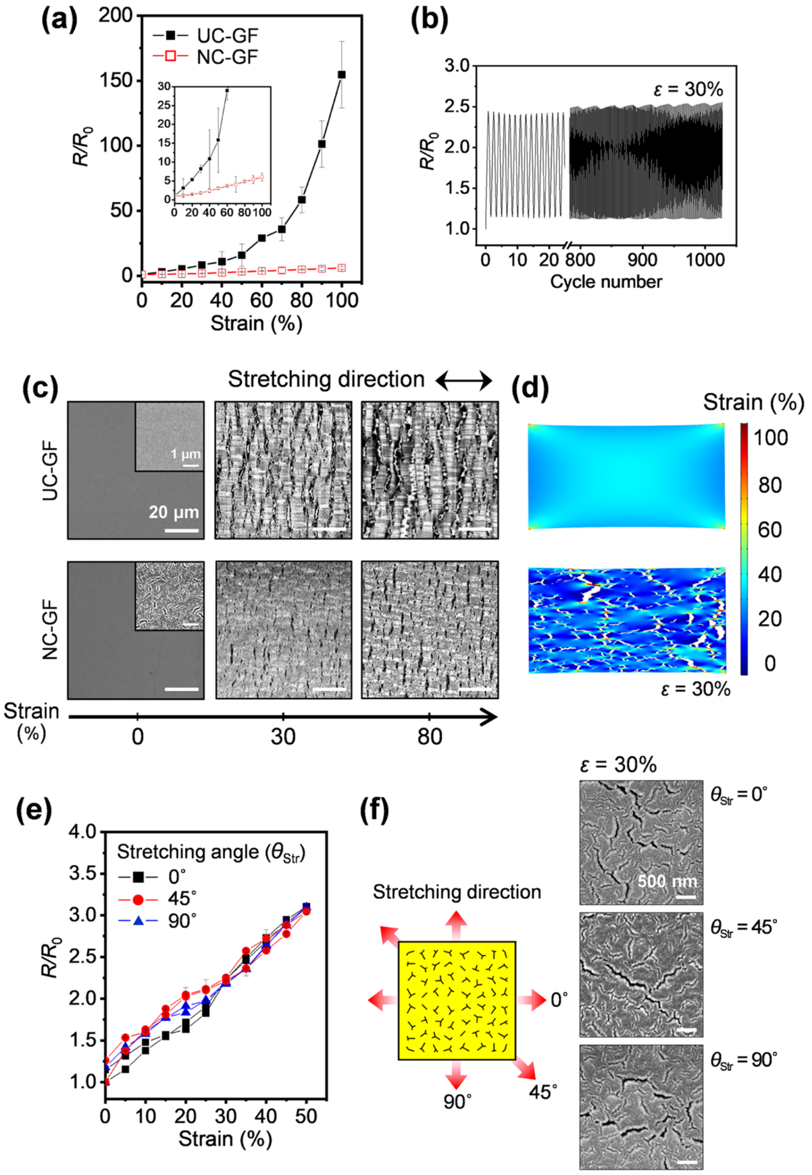

Figure 3. Electrical properties of gold films under stretching. (a) Electrical resistance change (R/R_0) as a function of tensile strain for the UC-GF and the NC-GF. (b) Cycle test for the NC-GF under 30% tensile strain. (c) SEM images showing the propagation of macroscale cracks under stretching for the UC-GF and the NC-GF. (d) Stress distribution of the UC-GF (top) and the NC-GF (bottom) under 30% stretching. (e) R/R_0 as a function of tensile strain for the NC-GF with different stretching angles. (f) Schematic illustration and the corresponding SEM images of the NC-GF under 30% tensile strain with different stretching angles.

swelling test (Figure S3) show that the as-prepared NC-GF exhibited good interfacial adhesion and robustness.

Nanocrack Formation Mechanism. Thermal evaporation leads to thermal residual stress σ_{th} on evaporated thin films;[34,35] however, typical metal thin films mostly do not develop cracks because σ_{th} is usually less than the critical tensile stress $\sigma_{tensile}$ of the film (Figure S4).[36] By contrast, our proposed method clearly induces the formation of nanocracks in the Au thin film without damaging the underlying PDMS (Figure S5). To identify the mechanism by which the nanocracks form during thermal evaporation, we observed how the morphology of the Au films varies with the stepwise variation of their thickness t_{Au}.

The nanocrack formation is proposed to occur in three steps—"bulging," "initiation," and "propagation"—as revealed by the corresponding images and height profiles (Figure 2a). The PDMS contains the residual solvent; when thermal evaporation begins (t_{Au} = 10 nm), the solvent agglomerates[37] and erupts, generating an externally directed force under the Au film so that bulges form in the film.[38] The driving force for the eruption of solvent is assumed to be the evaporation of the internal solvent due to the thermal energy that the deposited atoms transfer to the elastomeric substrate during thermal evaporation. This eruption imposes a large tensile stress σ_{erupt}; when the total applied stress $\sigma_{th} + \sigma_{erupt}$ exceeds the critical tensile stress $\sigma_{tensile}$ of Au, cracking occurs during the subsequent evaporation (t_{Au} = 20 nm) (see the estimation of σ_{erupt} and conditions for the film crack initiation of the film in the Supporting Information; Figures S6 and S7). To support our proposed mechanism, we deposited Au onto PDMS with an excessive amount of residual solvent and observed a crater-like morphology (Figure 2b). As the metal was deposited further (t_{Au} = 50 nm), the bulges disappeared, resulting in film smoothing,[39] followed by the development of uniform nanocracks from the initiated cracks.[40] On the basis of the aforementioned results, the

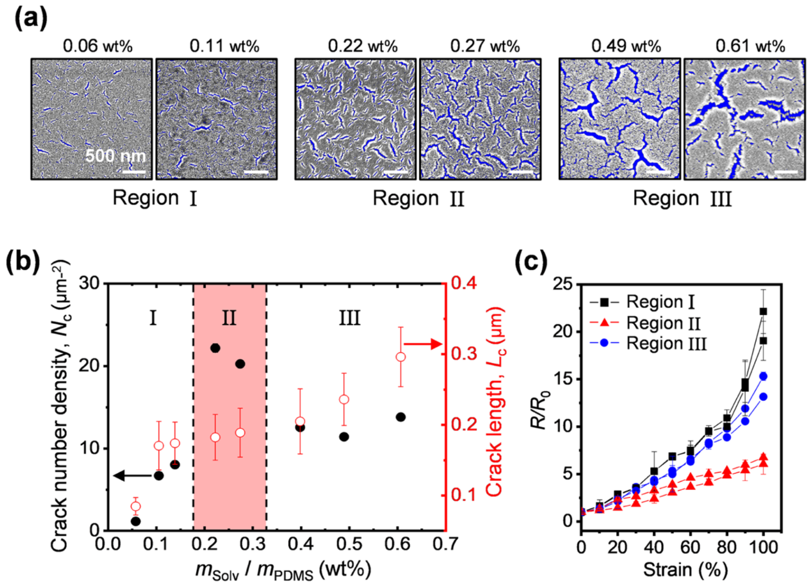

Figure 4. Control for the geometry of nanocracks. (a) SEM images of the NC-GF according to the amount of residual solvent. (b) Number density (N_c) and length (L_c) of nanocracks as a function of solvent content in the PDMS film. (c) R/R_0 as a function of tensile strain for the NC-GF varying with the geometry of nanocracks.

region where t_{Au} of 10 nm or less was classified as "bulging," 20–30 nm as "initiation," and 50 nm or more as "propagation." Notably, the nanocracks exhibited a radial shape because the eruption force applied to the underside of the film exhibited no preferred direction. A quantitative analysis using an angle-measurement program shows that the nanocracks were distributed uniformly over all directions (Figure 2c). Considering the radial growth of cracks and their omnidirectional distribution in the film, they are therefore referred to as "radial nanocracks" (Figure S8). Furthermore, a nanocracked silver film (NC-SF) and a nanocracked copper film (NC-CF) were fabricated by the solvent eruption method because the tensile strain is not dominantly affected by the types of metals (Figure 2d).

Mechanical and Electrical Stretchability. Compared with the UC-GF, the NC-GF exhibited better electrical characteristics under stretching (Figure 3a). The UC-GF showed an R/R_0 of 154.6 under 100% strain, and the R/R_0 as a function of ε became highly increased at $\varepsilon > 50\%$, rendering it almost useless for stretchable interconnects. By contrast, the NC-GF demonstrated stable operation in a stretched state, with an R/R_0 of 6.0 under 100% strain. In addition, the electrical resistance of this NC-GF electrode was almost stable under cycle tests at $\varepsilon = 30\%$ (Figure 3b), and damage to the film was insignificant (Figure S9). The improved stretchability was similarly applied to the NC-SF and the NC-CF (Figure S10).

To identify the mechanism of the improved stretchability, we compared the macroscale cracks of the UC-GF and the NC-GF in a stretched state because these cracks determine the connectivity of the current paths (Figures 3c and S11). The macroscale cracks of the UC-GF propagated transversely under stretching, so the current paths were disrupted and the electrical resistance increased greatly; this fracture behavior is typical for metal films on an elastomer because they have no stress-relaxation sites that can retard crack propagation.[41] By contrast, the macroscale cracks of the NC-GF propagated in a zigzag pattern, only slightly affecting the connectivity of the current path. These stretchability-enhancing effects of the preformed nanocracks are attributed to two aspects: First, the nanocracks can deflect macroscale cracks along the direction of the preformed nanocrack (Figure S12), resulting in a decrease in the stress intensity and propagation rate at the crack tips.[42] The presence of zigzag cracks in the NC-GF supports this speculation, which is consistent with the cracks in the NC-SF and the NC-CF (Figure S13). Second, the nanocracks can prevent the applied stress from concentrating in the center of a thin film by causing deformation and dissipation of stress in the vicinity of the cracks under stretching, thereby avoiding the formation of long transverse cracks in the film.[43] Mechanical simulations using COMSOL have verified that, under stretching, the applied stress concentrates on the nanocrack edges and is delocalized over the film (Figure 3d). The schematics in Figure S14 explain the overall mechanism of crack propagation on the NC-GF. Moreover, because of the uniform distribution of the radial nanocracks, the NC-GF exhibits almost identical electrical characteristics during stretching in the 0, 45, and 90° directions (Figure 3e); SEM images also support this omnidirectional stretchability (Figure 3f). These results demonstrate that our NC-GF is potentially useful in various applications in which the substrate is stretched in any direction; examples include wearable and attachable on-body devices.

Nanocrack Control. One of the great advantages of our method is that the stretchability of the NC-GF can be modulated by adjusting the nano-cracks' geometry, which is dependent on the solvent-induced tensile stress during thermal evaporation. To adjust the stress, the residual solvent content in PDMS was controlled by varying the cross-linking density and the prebaking time of the PDMS before thermal evaporation (Figure S15).

The morphological changes of the NC-GFs show that the nanocracks continued to grow with the increase of the residual solvent content (Figure 4a). To quantify the changes in the geometry of the growing nanocracks, we divided them into three regions (I, II, and III), depending on their number density N_c and length L_c (Figures 4b and S16). At low ratios between the mass of the solvent (m_{Solv}) and the mass of PDMS (m_{PDMS}) (i.e., $m_{Solv}/m_{PDMS} < 0.2$ wt %), the N_c and L_c were the lowest because the cracks had not substantially grown (region I). At moderate solvent contents (0.2 wt % < m_{Solv}/m_{PDMS} < 0.3 wt %), the

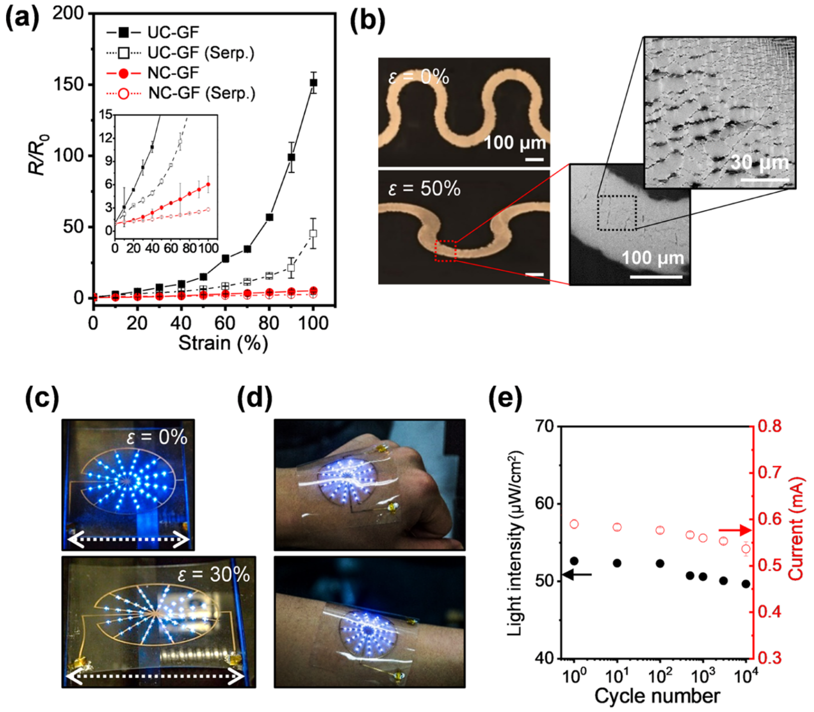

Figure 5. Application of serpentine patterns and stretchable interconnects for a radial LED array. (a) R/R_0 as a function of tensile strain for the UC-GF and the NC-GF with (dot) and without (line) the serpentine pattern. (b) OM and SEM images of the NC-GF with a serpentine pattern before and after stretching ($\varepsilon = 50\%$). (c) 4 × 12 radial LED array before and after stretching ($\varepsilon = 30\%$). (d) 4 × 12 radial LED array mounted on the human body. (e) Light intensity and current of a single LED under repeated tensile cycles.

solvent-induced tensile stress increased; thus, nanocracks with increased N_c and L_c were uniformly formed over a deposited film (region II). As the solvent content was increased further ($m_{\text{Solv}}/m_{\text{PDMS}} > 0.3$ wt %), the growing nanocracks merged together, resulting in a decrease in N_c and an increase in L_c (region III).

To investigate the geometrical effects of the nanocracks on the stretchability of the NC-GFs, we compared the dependence of R/R_0 on ε in the three aforementioned regions. Under 100% strain, the R/R_0 of the NC-GFs corresponding to region II was the lowest on average (Figure 4c). This result suggests that a high number density of short nanocracks is the most suitable geometry for stretching. Otherwise, the excessively short or long cracks with a low number density cannot function as stress distribution sites or they instead grow into macroscale defect sites in the film under stretching (Figure S17). These results demonstrate that the proposed approach provides a simple method to improve the stretchability of metal thin films by controlling the residual solvent content in the substrate and manipulating the geometry of the nanocracks.

Stretchable Interconnects. The stretchable NC-GF was fabricated via a single-step metal thermal evaporation process, so its electrical characteristics could be further improved by applying an extrinsic deformable geometry such as a serpentine pattern. In tensile tests, the serpentine pattern enhanced the electrical characteristics of the stretched Au films, and the R/R_0 of the serpentine NC-GF was reduced to 2.8 under 100% strain (Figure 5a). Although zigzag cracking occurred under 50% strain, the morphology of the film was well connected (Figure 5b). These electrical characteristics are highly superior compared to the previously reported thin-film metal electrodes fabricated by a single thermal evaporation process which show higher R/R_0 under stretching due to the absence of the optimized crack geometries.[44−46]

To verify the applicability of the NC-GF in soft electronics, we used thermal evaporation to fabricate a 4 × 12 stretchable interconnect with a radial shape on a PDMS film (Figure S18). The radial pattern was designed to demonstrate the omnidirectional electrical characteristics of the NC-GF. All the individual LEDs in the array operated well when the film was stretched in all directions (Figure 5c) and even when it was stretched on the curved human skin (Figure 5d). Quantitative analysis using a photodetector confirmed that the light emission of the LED changed little during a single stretching and compression cycle (Figure S19) and degraded only slightly under repeated cycling at 30% strain (Figure 5e). These results demonstrate that our simple process for manufacturing omnidirectionally stretchable and robust electrodes is sufficiently versatile for use in practical soft applications such as flexible sensors and health-monitoring devices.

CONCLUSIONS

We exploited a solvent-eruption phenomenon to fabricate stretchable and robust metal thin films with radially formed nanocracks on elastomeric substrates. When fabricated by simultaneous surface thiolation of the elastomeric substrate, the NC-GF exhibited highly improved stretchability and robustness compared with a conventional gold film. The results of morphological observations and mechanical simulations showed that the radial nanocracks delocalized the stress and thereby helped to retard the propagation of the macroscale crack under omnidirectional stretching. In addition, it was possible to control the nanocrack topographies through variation of the residual solvent content, and the stretching tendency of the NC-GF for different crack geometries suggested that a high number density of short nanocracks was the most suitable geometry for stretching. Last, the feasibility of the NC-GF in soft electronics was verified by manufacturing stretchable interconnects for a radial LED array; the array operated stably during stretching and cycle tests. From these results, our method shows that a stretchable and robust metal film that can be used for practical applications was fabricated on an elastomeric substrate using a metal thermal evaporation process, which is versatile in that it is a simple and widely used technology. Furthermore, our nanocrack fabrication method can be applied to a variety of metals and elastomeric substrates because the crack formation can be controlled by modulation of the residual solvent. We expect that our approach will provide a new method toward the practical development of future flexible and stretchable electronics.

EXPERIMENTAL SECTION

Chemicals. All organic solvents and MPTMS used in this work were of anhydrous grade and purchased from Sigma-Aldrich. The PDMS (Sylgard 184) prepolymer and the cross-linker were purchased from Dow Chemical Co.

Preparation of the PDMS Substrate with the Residual Solvent and Thiol Group-Ended Silane. The PDMS mixture [PDMS prepolymer/cross-linker = 3:1, 10:1, and 20:1 (w/w)] was poured onto a glass slide. The mixture was soft-cured and planarized at room temperature (RT) for 10 h and then hard-cured at 65 °C for 3 h. The PDMS film (220−250 μm thickness) was immersed in hexane for 1 h at RT; hexane has high compatibility and solubility in PDMS; therefore, it is used to impregnate the PDMS film. The PDMS film was removed from hexane and then washed with hexane and ethanol to remove the PDMS oligomer that seeped from the PDMS matrix. The process of thiolation is similar to the previous solvent process. The cured PDMS film was treated for 25 min with ultraviolet-ozone, immersed in 2 mM MPTMS dissolved in hexane for 1 h at RT, and then washed with hexane and ethanol. Next, the film was thermally baked at 120 °C for 10 min, sonicated in hexane for 3 min, and then rinsed with ethanol. The overall process was carried out with reference to the practical thiolation methods.[47,48] The washed PDMS film was dried at 120 °C in a convection oven for 3 min to modulate the amount of the residual solvent that it retained. The amount of residual solvent within the film was measured using a microbalance (XP6, Mettler Toledo) and thermogravimetric analysis (Q50, TA Instruments Inc.).

Vacuum Application and Thermal Evaporation. Before the start of the thermal evaporation, the prepared PDMS film was loaded onto the sample stage and kept in the vacuum chamber. To ensure a constant amount of residual solvent within the PDMS film, the vacuum conditions of the evaporator were precisely controlled. First, the vacuum chamber was kept at $\sim 2.0 \times 10^{-6}$ Torr for 3 h to eliminate the effects of pretime evaporation. Then, the PDMS sample was kept under low vacuum for 10 min until the pressure reached 2.0×10^{-3} Torr and held for 3 min. Then, high vacuum was applied for 35 min until the pressure reached 3.0×10^{-6} Torr and then held at that pressure for 15 min. Upon completing the vacuum application, Au, Ag, or Cu was thermally evaporated to a thickness of 50 nm at a deposition rate of 0.1−0.2 Å/s until 10 nm thickness and at 0.6−0.7 Å/s until 50 nm thickness on the PDMS film.

Preparation of the Gold Film with a Crater-like Morphology. The prepared PDMS sample [prepolymer/cross-linker, 20:1 (w/w)] without prebaking was kept under high vacuum for 35 min in the chamber. Then, without the 15 min holding time at the pressure of 3.0×10^{-6} Torr (the solvent content $m_{\mathrm{Solv}}/m_{\mathrm{PDMS}}$ is about 0.7−0.9 wt %), Au was thermally evaporated to a thickness of 50 nm at a deposition rate of 0.1−0.2 Å/s until 10 nm thickness and at 0.6−0.7 Å/s until 50 nm thickness on the PDMS film.

Crack Characterization. The morphologies of the cracks were characterized using a field-emission scanning electron microscope (Hitachi S-4200), and an atomic force microscope (Digital Instruments Multimode) operated in the tapping mode. The geometries of cracks were analyzed using ImageJ and Adobe Photoshop software. The pixels of each crack were automatically designed, and their lengths, angles, and number densities were counted manually.

Electrical Property Characterization. All the electrical properties of the electrodes were characterized by a two-terminal measurement using a Keithley 4200 instrument. Copper wires (Puratronic copper, 0.1 mm thickness) were connected to the electrode pattern (width: 1 mm) at a distance of 10 mm, and the eutectic gallium−indium (EGaIn, Alfa Aesar, 99% metal basis) liquid metal was applied to the electrode/wire interface to ensure the ohmic contact. The stretching test was conducted using a motion controller (Autonics Co., PMC-2HS 2-Axis Motion controller).

FT-IR Spectroscopy. The infrared spectra of the thiol groups that had been applied to the silicon wafer and the PDMS film were recorded using a Fourier transform infrared spectrometer (Bruker Co., Vertex 70v) in attenuated total reflectance mode.

LED Operation and Light Intensity Measurements. Commercially available blue LEDs (1 mm × 0.6 mm × 0.2 mm) were purchased from Rohm Semiconductor (755-SMLP13BC8TT86). The LED was operated with 3 V and 220 W applied by a DC power supply. An optical power meter (Newport Co., 1918-R) was used to measure the light intensity of the LEDs. The distance between the detector and the LEDs was maintained at 3 cm.

ASSOCIATED CONTENT

Supporting Information

The Supporting Information is available free of charge at https://pubs.acs.org/doi/10.1021/acsanm.0c01536.

> Equations for thermal stress applied to a gold film during vacuum deposition and critical tensile stress of the deposited gold film; grain size of the gold film, solubility parameter, and mixing enthalpy of PDMS and organic solvents; morphology of the NC-GF varying with solvent type; sheet resistance of the UC-GF and the NC-GF; stability test of the gold film in a swelling solvent; growth of the UC-GF; side and bottom morphologies of the NC-GF; radial growth of the NC-GF; morphology of the UC-GF and the NC-GF after the cycle test; stretchable test of the NC-SF and the NC-CF; nanocrack propagation in the NC-GF; macroscale crack propagation in the UC-GF and the NC-GF; macroscale crack propagation in the NC-SF and the NC-CF; schematic illustration of the crack propagation in the NC-GF; amount of residual solvent in the PDMS varying with time; morphology of the NC-GF varying with the prebaking time and the cross-linking density of the PDMS and the geometrical statistics of the nanocracks; macroscale crack propagation of the NC-GF with a high amount of residual solvent (region III); stretchable interconnects for a radial LED array; and photographs of a single LED varying with applied strain in the stretched and compressed states (PDF)
>
> Stretching test for a single LED under 30% strain (MP4)
>
> Compression test for a single LED under 30% strain (MP4)

AUTHOR INFORMATION

Corresponding Authors

Seung Goo Lee − *Department of Chemistry, University of Ulsan, Ulsan 44610, Korea*; Email: lees9@ulsan.ac.kr

Kilwon Cho − *Department of Chemical Engineering and Center for Advanced Soft Electronics, Pohang University of Science and Technology, Pohang 37673, Korea*; orcid.org/0000-0003-0321-3629; Email: kwcho@postech.ac.kr

Authors

Seong Won Kim − *Department of Chemical Engineering and Center for Advanced Soft Electronics, Pohang University of Science and Technology, Pohang 37673, Korea*

Siyoung Lee − *Department of Chemical Engineering and Center for Advanced Soft Electronics, Pohang University of Science and Technology, Pohang 37673, Korea*

Daegun Kim − *Department of Chemical Engineering and Center for Advanced Soft Electronics, Pohang University of Science and Technology, Pohang 37673, Korea*

Complete contact information is available at:
https://pubs.acs.org/10.1021/acsanm.0c01536

Author Contributions

S.W.K., S.G.L., and K.C. conceived the project and S.W.K. designed and performed the experiments and collected the data. All the authors analyzed and discussed the data and have given their approval to the final version of the manuscript.

Notes

The authors declare no competing financial interest.

■ ACKNOWLEDGMENTS

This work was supported by a grant (code no. 2012M3A6A5055728) from the Center for Advanced Soft Electronics under the Global Frontier Research Program of the Ministry of Science, ICT, Korea.

■ REFERENCES

(1) Lee, E.; Lee, S. G.; Cho, K. Direct growth of substrate-adhered graphene on flexible polymer substrates for soft electronics. *Chem. Mater.* **2019**, *31*, 4451−4459.

(2) Papadopoulos, N.; Qiu, W.; Ameys, M.; Smout, S.; Willegems, M.; Deroo, F.; van der Steen, J.-L.; Kronemeijer, A. J.; Dehouwer, M.; Mityashin, A.; Gehlhaar, R.; Myny, K. Touchscreen tags based on thin-film electronics for the Internet of Everything. *Nat. Electron.* **2019**, *2*, 606−611.

(3) Sekitani, T.; Nakajima, H.; Maeda, H.; Fukushima, T.; Aida, T.; Hata, K.; Someya, T. Stretchable active-matrix organic light-emitting diode display using printable elastic conductors. *Nat. Mater.* **2009**, *8*, 494−499.

(4) Zhang, W.; Guo, R.; Sun, J.; Dang, L.; Liu, Z.; Lei, Z.; Sun, Q. Textile carbon network with enhanced areal capacitance prepared by chemical activation of cotton cloth. *J. Colloid Interface Sci.* **2019**, *553*, 705−712.

(5) Yeo, J. C.; Yap, H. K.; Xi, W.; Wang, Z.; Yeow, C.-H.; Lim, C. T. Flexible and stretchable strain sensing actuator for wearable soft robotic applications. *Adv. Mater. Technol.* **2016**, *1*, 1600018.

(6) You, I.; Kim, B.; Park, J.; Koh, K.; Shin, S.; Jung, S.; Jeong, U. Stretchable E-Skin Apexcardiogram Sensor. *Adv. Mater.* **2016**, *28*, 6359.

(7) Yan, C.; Wang, J.; Wang, X.; Kang, W.; Cui, M.; Foo, C. Y.; Lee, P. S. An intrinsically stretchable nanowire photodetector with a fully embedded structure. *Adv. Mater.* **2014**, *26*, 943−950.

(8) Bae, G. Y.; Pak, S. W.; Kim, D.; Lee, G.; Kim, D. H.; Chung, Y.; Cho, K. Linearly and highly pressure-sensitive electronic skin based on a bioinspired hierarchical structural array. *Adv. Mater.* **2016**, *28*, 5300.

(9) Lee, S.; Kim, J.; Yun, I.; Bae, G. Y.; Kim, D.; Park, S.; Yi, I.; Moon, W.; Chung, Y.; Cho, K. An ultrathin conformable vibration-responsive electronic skin for quantitative vocal recognition. *Nat. Commun.* **2019**, *10*, 2468.

(10) Baek, S.; Bae, G. Y.; Kwon, J.; Cho, K.; Jung, S. Flexible pressure-sensitive contact transistors operating in the subthreshold regime. *ACS Appl. Mater. Interfaces* **2019**, *11*, 31111−31118.

(11) Bae, G. Y.; Han, J. T.; Lee, G.; Lee, S.; Kim, S. W.; Park, S.; Kwon, J.; Jung, S.; Cho, K. Pressure/temperature sensing bimodal electronic skin with stimulus discriminability and linear sensitivity. *Adv. Mater.* **2018**, *30*, 1803388.

(12) Ma, R.; Chou, S.-Y.; Xie, Y.; Pei, Q. Morphological/nanostructural control toward intrinsically stretchable organic electronics. *Chem. Soc. Rev.* **2019**, *48*, 1741−1786.

(13) Xu, F.; Zhu, Y. Highly conductive and stretchable silver nanowire conductors. *Adv. Mater.* **2012**, *24*, 5117−5122.

(14) Lee, G.; Lee, S. G.; Chung, Y.; Bae, G. Y.; Lee, S.; Ryu, S.; Cho, K. Omnidirectionally and highly stretchable conductive electrodes based on noncoplanar zigzag mesh silver nanowire arrays. *Adv. Electron. Mater.* **2016**, *2*, 1600158.

(15) Guo, C. F.; Sun, T.; Liu, Q.; Suo, Z.; Ren, Z. Highly stretchable and transparent nanomesh electrodes made by grain boundary lithography. *Nat. Commun.* **2014**, *5*, 3121.

(16) Wang, Y.; Liu, Q.; Zhang, J.; Hong, T.; Sun, W.; Tang, L.; Arnold, E.; Suo, Z.; Hong, W.; Ren, Z.; Guo, C. F. Giant Poisson's Effect for Wrinkle-Free Stretchable Transparent Electrodes. *Adv. Mater.* **2019**, *31*, 1902955.

(17) Sunwoo, S. H.; Han, S. I.; Kang, H.; Cho, Y. S.; Jung, D.; Lim, C.; Lim, C.; Cha, M. j.; Lee, S. P.; Hyeon, T.; Kim, D. H. Stretchable low-impedance nanocomposite comprised of ag−au core−shell nanowires and Pt black for epicardial recording and stimulation. *Adv. Mater. Technol.* **2019**, *5*, 1900768.

(18) Jang, K.; Li, K.; Chung, H. U.; Xu, S.; Jung, H. N.; Yang, Y.; Kwak, J. W.; Jung, H. H.; Song, J.; Yang, C.; Wang, A.; Liu, Z.; Lee, J. Y.; Kim, B. H.; Kim, J.; Lee, J.; Yu, Y.; Kim, B. J.; Jang, H.; Yu, K. J.; Kim, J.; Lee, J. W.; Jeong, J.; Song, Y. M.; Huang, Y.; Zhang, Y.; Rogers, J. A. Self-assembled three dimensional network designs for soft electronics. *Nat. Commun.* **2017**, *8*, 15894.

(19) Luo, N.; Ding, J.; Zhao, N.; Leung, B. H. K.; Poon, C. C. Y. Mobile Health: Design of Flexible and Stretchable Electrophysiological Sensors for Wearable Healthcare Systems. *International Conference on Wearable and Implantable Body Sensor Networks 2014, Jun 16−19*, 2014; pp 87−91.

(20) Moore, G. E. Cramming more components onto integrated circuits. *Electronics* **1965**, *38*, 114−117.

(21) Ma, Y.; Jang, K.-I.; Wang, L.; Jung, H. N.; Kwak, J. W.; Xue, Y.; Chen, H.; Yang, Y.; Shi, D.; Feng, X.; Rogers, J. A.; Huang, Y. Design of strain-limiting substrate materials for stretchable and flexible electronics. *Adv. Funct. Mater.* **2016**, *26*, 5345−5351.

(22) Yu, S.; Han, H. J.; Kim, J. M.; Yim, S.; Sim, D. M.; Lim, H.; Lee, J. H.; Park, W. I.; Park, J. H.; Kim, K. H.; Jung, Y. S. Area-selective lift-off mechanism based on dual-triggered interfacial adhesion switching: highly facile fabrication of flexible nanomesh electrode. *ACS Nano* **2017**, *11*, 3506−3516.

(23) Liu, N.; Chortos, A.; Lei, T.; Jin, L.; Kim, T. R.; Bae, W.-G.; Zhu, C.; Wang, S.; Pfattner, R.; Chen, X.; Sinclair, R.; Bao, Z. Ultra-transparent and stretchable graphene electrodes. *Sci. Adv.* **2017**, *3*, No. e1700159.

(24) Hu, H.; Wang, S.; Wang, S.; Liu, G.; Cao, T.; Long, Y. Aligned silver nanowires enabled highly stretchable and transparent electrodes with unusual conductive property. *Adv. Funct. Mater.* **2019**, *29*, 1902922.

(25) Kang, D.; Pikhitsa, P. V.; Choi, Y. W.; Lee, C.; Shin, S. S.; Piao, L.; Park, B.; Suh, K.-Y.; Kim, T.-i.; Choi, M. Ultrasensitive mechanical crack-based sensor inspired by the spider sensory system. *Nature* **2014**, *516*, 222−226.

(26) Yang, T.; Li, X.; Jiang, X.; Lin, S.; Lao, J.; Shi, J.; Zhen, Z.; Li, Z.; Zhu, H. Structural engineering of gold thin films with channel cracks for ultrasensitive strain sensing. *Mater. Horiz.* **2016**, *3*, 248−255.

(27) Lacour, S. P.; Chan, D.; Wagner, S.; Li, T.; Suo, Z. Mechanisms of reversible stretchability of thin metal films on elastomeric substrates. *Appl. Phys. Lett.* **2006**, *88*, 204103.

(28) Minev, I. R.; Musienko, P.; Hirsch, A.; Barraud, Q.; Wenger, N.; Moraud, E. M.; Gandar, J.; Capogrosso, M.; Milekovic, T.; Asboth, L.; Torres, R. F.; Vachicouras, N.; Liu, Q.; Pavlova, N.; Duis, S.; Larmagnac, A.; Voros, J.; Micera, S.; Suo, Z.; Courtine, G.; Lacour, S. P. Electronic dura mater for long-term multimodal neural interfaces. *Science* **2015**, *347*, 159−163.

(29) Yang, C.; Yu, M.; Wang, C.; Yu, Z. Facile fabrication of highly stretchable nanocrack silver film using magnetron sputtering. *IOP Conf. Ser.: Mater. Sci. Eng.* **2017**, *265*, 012008.

(30) Baëtens, T.; Pallecchi, E.; Thomy, V.; Arscott, S. Cracking effects in squashable and stretchable thin metal films on PDMS for flexible microsystems and electronics. *Sci. Rep.* **2018**, *8*, 9492.

(31) Matsuhisa, N.; Jiang, Y.; Liu, Z.; Chen, G.; Wan, C.; Kim, Y.; Kang, J.; Tran, H.; Wu, H. C.; You, I.; Bao, Z.; Chen, X. High-transconductance stretchable transistors achieved by controlled gold microcrack morphology. *Adv. Electron. Mater.* **2019**, *5*, 1900347.

(32) Wilson, L.; Head, J. W. Lunar floor-fractured craters: Modes of dike and sill emplacement and implications of gas production and intrusion cooling on surface morphology and structure. *Icarus* **2018**, *305*, 105−122.

(33) Lee, J. N.; Park, C.; Whitesides, G. M. Solvent compatibility of poly(dimethylsiloxane)-based microfluidic devices. *Anal. Chem.* **2003**, *75*, 6544−6554.

(34) Bowden, N.; Brittain, S.; Evans, A. G.; Hutchinson, J. W.; Whitesides, G. M. Spontaneous formation of ordered structures in thin films of metals supported on an elastomeric polymer. *Nature* **1998**, *393*, 146−149.

(35) Akogwu, O.; Kwabi, D.; Munhutu, A.; Tong, T.; Soboyejo, W. O. Adhesion and cyclic stretching of Au thin film on poly(dimethylsiloxane) for stretchable electronics. *J. Appl. Phys.* **2010**, *108*, 123509.

(36) Chen, Y.; Wu, Y.; Mechael, S. S.; Carmichael, T. B. Heterogeneous surface orientation of solution-deposited gold films enables retention of conductivity with high strain- a new strategy for stretchable electronics. *Chem. Mater.* **2019**, *31*, 1920−1927.

(37) Watanabe, H.; Suzuki, M.; Inaoka, H.; Ito, N. Ostwald ripening in multiple-bubble nuclei. *J. Chem. Phys.* **2014**, *141*, 234703.

(38) Seagraves, A. N.; Radovitzky, R. A. An analytical theory for radial crack propagation: application to spherical indentation. *J. Appl. Mech.* **2013**, *80*, 041018.

(39) McNeil, J. R.; Wei, L. J.; Al-Jumaily, G. A.; Shakir, S.; Mclver, J. K. Surface smoothing effects of thin film deposition? *Appl. Opt.* **1985**, *24*, 480−485.

(40) Seghir, R.; Arscott, S. Controlled mud-crack patterning and self-organized cracking of polydimethylsiloxane elastomer surfaces. *Sci. Rep.* **2015**, *5*, 14787.

(41) Douville, N. J.; Li, Z.; Takayama, S.; Thouless, M. D. Fracture of metal coated elastomers. *Soft Matter* **2011**, *7*, 6493−6500.

(42) Suresh, S. Micromechanisms of fatigue crack growth retardation following overloads. *Eng. Fract. Mech.* **1983**, *18*, 577−593.

(43) Holl, M.; Loehnert, S.; Wriggers, P. An adaptive multiscale method for crack propagation and crack coalescence. *Int. J. Numer. Meth. Eng.* **2013**, *93*, 23−51.

(44) Graz, I. M.; Cotton, D. P. J.; Lacour, S. P. Extended cyclic uniaxial loading of stretchable gold thin-films on elastomeric substrates. *Appl. Phys. Lett.* **2009**, *94*, 071902.

(45) Sun, J.-Y.; Lee, H.-R.; Oh, K. H. Columnar grown copper films on polyimides strain beyond 100%. *Sci. Rep.* **2015**, *5*, 13791.

(46) Putz, B.; Schoeppner, R. L.; Glushko, O.; Bahr, D. F.; Cordill, M. J. Improved electro-mechanical performance of gold films on polyimide without adhesion layers. *Scr. Mater.* **2015**, *102*, 23−26.

(47) Gothe, P. K.; Gaur, D.; Achanta, V. G. MPTMS self-assembled monolayer deposition for ultra-thin gold films for plasmonics. *J. Phys. Commun.* **2018**, *2*, 035005.

(48) Osmani, B.; Deyhle, H.; Weiss, F. M.; Topper, T.; Karapetkova, M.; Leung, V.; Muller, B. Morphology and conductivity of Au films on polydimethylsiloxane using (3-mercaptopropyl)trimethoxysilane as adhesion promoter. *Proc. of SPIE* **2016**, *9798*, 979822.